Prompt Optimization Meets Subspace Representation Learning for Few-shot Out-of-Distribution Detection

Anonymous authors
Paper under double-blind review

Abstract

The reliability of artificial intelligence (AI) systems in open-world settings depends heavily on their ability to flag out-of-distribution (OOD) inputs unseen during training. Recent advances in large-scale vision-language models (VLMs) have enabled promising few-shot OOD detection frameworks using only a handful of in-distribution (ID) samples. However, existing prompt learning-based OOD methods largely overlook the geometry of the visual feature embeddings learned by VLMs whose structure is particularly informative for distinguishing ID from OOD data and holds rich representation capacity as they are pre-trained on millions of samples. To address this, we introduce a *geometry-aware context optimization framework* that integrates subspace representation learning with prompt tuning. By projecting ID-relevant features into a subspace spanned by prompt vectors and simultaneously projecting ID-irrelevant components via orthogonal null-space projections, our approach strengthens the discriminative power of the learned prompt vectors, thereby leading to enhanced ID–OOD separability at test time. To enable an easy-to-handle, end-to-end learning under this framework, we design a geometry-regularized learning criterion that ensures strong OOD detection performance as well as high ID classification accuracy across settings. Moreover, the proposed framework can be seamlessly integrated with a wide range of existing context optimization methods, effectively complementing their softmax-based OOD detectors. Experiments on various real-world datasets showcase the effectiveness of our approach for reliable open-world AI systems.

1 Submission of papers to TMLR

2 Introduction

Deep learning models often exhibit overconfidence when exposed to inputs from unseen, out-of-distribution (OOD) categories (Goodfellow et al., 2014). Such overconfidence can lead to critical failures in open-world and safety-sensitive applications such as autonomous driving (Geiger et al., 2012) and medical diagnostics (Schlegl et al., 2017). These risks have spurred substantial interest in OOD detection approaches, that aim to equip models with the ability to reliably detect OOD inputs that falls outside the known class (Yang et al., 2024a). Traditional OOD detection approaches (Liu et al., 2020a; Huang et al., 2021; Lee et al., 2018; Huang & Li, 2021) typically rely on designing scoring functions or incorporating auxiliary outlier datasets during training. While such methods have demonstrated promise in controlled settings, they often fail to generalize in dynamic, real-world environments where the nature of the OOD data is unpredictable (Shen et al., 2024; Kirichenko et al., 2020; Fang et al., 2025).

Recently, large-scale vision-language models (VLMs) such as contrastive language-image pretraining (CLIP) (Radford et al., 2021) have shown strong zero-shot performance on downstream tasks by aligning visual and textual modalities in a shared embedding space. This opens a new direction for OOD detection, particularly in low-resource or few-shot settings (Esmaeilpour et al., 2022; Ming et al., 2022; Miyai et al., 2023b). However, CLIP's zero-shot approach depends heavily on manually crafted prompts, where even slight variations (e.g., "*a flower*" vs. "*a type of a flower*") can significantly impact performance (Yuksekgonul et al., 2022; Nie et al., 2024). To reduce this sensitivity, a class of prompt tuning methods called

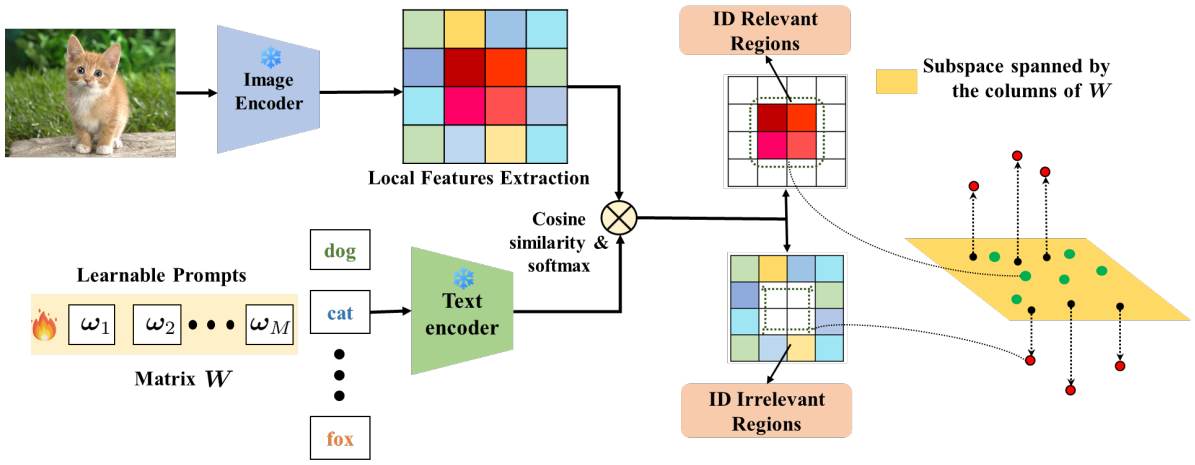

Figure 1: The proposed **Sub**space learning-based **Co**ntext **Op**timization (SubCoOp) framework for prompt-learning-based OOD detection.

context optimization has been introduced. For example, CoOp (Zhou et al., 2022b) and CoCoOp (Zhou et al., 2022a) replace hand-crafted textual embeddings with learnable context vectors that are optimized to enhance alignment between in-distribution (ID) image features and class text embeddings, leading to improved classification accuracy.

However, context optimization methods face a significant limitation in their direct applicability towards OOD detection tasks. By focusing on bringing ID image features closer to their text embeddings, these methods risk inadvertently incorporating background clutter or semantically irrelevant regions—some of which may actually represent OOD samples—into the ID representation space. This eventually weakens the model's ability to accurately distinguish between ID and OOD samples at test time. As a result, several subsequent approaches have introduced *proxy-OOD supervision* to explicitly guide models in learning more robust boundaries between ID and OOD samples (Miyai et al., 2023a; Yu et al., 2024; Xu et al., 2025). For instance, LoCoOp (Miyai et al., 2023a) addresses this limitation by leveraging CLIP's spatially-aware local features. It identifies ID-irrelevant regions—those where the true class is not among the top predictions—and treats them as proxy OOD features. By applying an entropy-maximization strategy to the predictions associated with ID-irrelevant features, this approach enhances the separation between ID and OOD samples without relying on any specific OOD data. A related method was proposed in (Yu et al., 2024), where adaptive weighting is incorporated into the LoCoOp optimization framework to dynamically balance ID- and OOD-specific loss terms based on the model's prediction confidence. Another prompt-tuning approach Zeng et al. (2024) combined global prompt-guided negative augmentation with local prompt-enhanced regional regularization to improve the OOD detection performance. Nonetheless, the approach relies on extensive data augmentation and is more computationally expensive as it separately learns class-wise local prompts and introduces negative prompts as well. Recently, the approach in (Xu et al., 2025) extends proxy-OOD supervision idea by incorporating pre-trained segmentation models for image inpainting to generate more informative proxy-OOD samples during few-shot training. Nevertheless, integrating this method into few-shot training is prohibitively expensive, requiring roughly 4–5 times longer training compared to other proxy-OOD supervision approaches (Miyai et al., 2023a; Yu et al., 2024), primarily due to the inpainting demands on the training dataset.

Our contributions. In this work, we aim to enhance the OOD detection capabilities of the existing context optimization methods by efficiently extracting more informative proxy-OOD supervision through geometry-aware prompt tuning from the pretrained visual-textual CLIP encoder under a limited training sample budget. Existing prompt learning approaches, through their cosine similary-based cross-entropy loss training, primarily shape the relative geometry among ID classes, but nonetheless overlook the discriminative geometry between ID and OOD features. Towards this, we introduce a novel framework that explicitly leverages the inherently discriminative geometry of the visual feature embeddings of the ID and OOD features. As prompt

vectors are the only learnable parameters in such frameworks, our key idea is to inject feature geometry-aware discriminative cues into their learning, thereby improving the ID-OOD separability at test time. Our key contributions are summarized as follows:

(i). To learn geometry-aware prompt vectors, we introduce subspace representation learning-based framework by projecting the ID features into a subspace spanned by the prompt vectors, while simultaneously projecting ID-irrelevant features into the orthogonal null space. This subspace-based formulation is designed to exploit a discriminative geometry between ID and OOD samples.

(ii). We design an easy-to-implement, subspace regularization loss that can be seamlessly integrated within context optimization, thereby enhancing the OOD detection performance without compromising the ID classification accuracy and without incurring any significant computational cost.

(iii). Experiments on large-scale real-world datasets such as ImageNet-1k (Deng et al., 2009) demonstrate that our method outperforms many state-of-the-art context optimization approaches for OOD detection and consistently performs well across diverse challenging settings.

3 Problem Statement

Consider an ID dataset $\mathcal{D}^{\text{in}} = \{(\mathbf{x}, y)\}$, where $\mathbf{x} \in \mathbb{R}^L$ denotes the input features of an image and $y \in \mathcal{Y}^{\text{in}} := \{1, \dots, K\}$ is its corresponding class label (also referred to as the *true label*). AI models are typically trained under the closed-world assumption, where test samples are expected to come from the same distribution as the ID data. In practice, however, models frequently encounter OOD samples—data that deviates from the training distribution (Hendrycks & Gimpel, 2016). In classification settings, there may occur a semantic-shift such that test samples may belong to an *unknown* label space $\mathcal{Y}^{\text{out}}$, where $\mathcal{Y}^{\text{in}} \cap \mathcal{Y}^{\text{out}} = \emptyset$. The objective of OOD detection is to build a classifier that, given a test sample $\mathbf{x}$, predicts whether it belongs to an ID class or not, thereby preventing models from assigning high-confidence predictions to OOD samples. OOD detection can be framed as a binary classification problem. Formally, this is achieved through a detection function $\boldsymbol{d}_\eta : \mathbb{R}^L \to \{\mathsf{ID}, \mathsf{OOD}\}$ such that

$$\boldsymbol{d}_\eta(\mathbf{x}) = \begin{cases} \mathsf{ID} & s(\mathbf{x}) \geq \eta \\ \mathsf{OOD} & s(\mathbf{x}) < \eta, \end{cases} \tag{1}$$

where $s(\mathbf{x})$ is a scoring function associated with the input feature $\mathbf{x}$ and η is the threshold.

Context Optimization with Learnable Prompts. Context optimization (CoOp) (Zhou et al., 2022b) leverages pre-trained VLMs, such as CLIP (Radford et al., 2021), for open-vocabulary visual recognition tasks. While CLIP typically uses static, hand-crafted prompts, CoOp learns a set of positive prompt vectors in a data-driven manner. These vectors are optimized as part of the model parameters during training, enabling few-shot learning for the downstream task.

Consider the ID input image $\mathbf{x} \in \mathbb{R}^L$, which is inputted to the visual encoder $f : \mathbb{R}^L \to \mathbb{R}^D$ of CLIP to extract the visual feature vector $f^{\text{in}} = f(\mathbf{x})$. The textual prompt is composed as $\boldsymbol{t}_k = \{\boldsymbol{\omega}_1, \boldsymbol{\omega}_2, \dots, \boldsymbol{\omega}_M, \boldsymbol{c}_k\}$, where each $\boldsymbol{\omega}_m \in \mathbb{R}^D$ is a learnable context vector, $\boldsymbol{c}_k \in \mathbb{R}^D$ is the class name embedding of the image, for each class $k \in [K]$, and M is the number of prompt vectors. The textual encoder $\boldsymbol{g}$ processes the prompt $\boldsymbol{t}_k$ to yield the textual feature $\mathbf{g}_k = \mathbf{g}(\boldsymbol{t}_k)$ (e.g., using a Transformer-based model). With these notations, we can represent the class prediction probabilities $\mathsf{Pr}(y = k \mid \mathbf{x})$ as follows:

$$\mathsf{Pr}(y = k \mid \mathbf{x}) = \frac{\exp\left(\text{sim}(f^{\text{in}}, \mathbf{g}_k)/\tau\right)}{\sum_{k'=1}^{K} \exp\left(\text{sim}(f^{\text{in}}, \mathbf{g}_{k'})/\tau\right)}, \tag{2}$$

where $\text{sim}(\cdot, \cdot)$ denotes the cosine similarity and $\tau > 0$ is a temperature parameter. Consequently, CoOp optimizes the prompt vectors using the cross-entropy loss by matching the class predictions in equation 2 and the true label y, i.e., $\mathcal{L}_{\text{CE}} = -\sum_{k=1}^{K} \mathbb{I}[y = k] \log \mathsf{Pr}(y = k \mid \mathbf{x})$. Although CoOp aligns the ID image with its class text embedding $\mathbf{g}_k$ in this manner, it inadvertently brings the text embedding closer to background or ID-irrelevant features with the ID image, resulting in incorrectly high confidence scores for OOD images

during test time. Hence, without access to OOD samples during training, the model struggles to learn a well-defined ID-OOD boundary for reliable OOD detection.

OOD Local Features Extraction. Recently, LoCoOp (Miyai et al., 2023a) introduced a novel perspective to prompt optimization-based OOD detection by extracting local features that serve as proxy OOD signals, thereby preventing the model from assigning high ID confidence scores to OOD-like features. To detect local features not corresponding to ID classes (i.e., ID-irrelevant features), the method in (Miyai et al., 2023a) examine a set of spatial indices from the feature map: $\mathcal{I} = \{0, 1, 2, \ldots, H \times W - 1\}$, where H and W are the height and width of the feature map, respectively. Following a strategy inspired by semantic segmentation (Radford et al., 2021), the class probabilities associated to each region $i \in \mathcal{I}$ can be computed based on the similarity between local visual features and text embeddings:

$$\mathsf{Pr}_i(y = k \mid \boldsymbol{x}) = \frac{\exp\left(\mathrm{sim}(\boldsymbol{f}_i^{\mathrm{in}}, \boldsymbol{g}_k)/\tau\right)}{\sum_{k'=1}^{K} \exp\left(\mathrm{sim}(\boldsymbol{f}_i^{\mathrm{in}}, \boldsymbol{g}_{k'})/\tau\right)}, \tag{3}$$

where $\boldsymbol{f}_i^{\mathrm{in}} \in \mathbb{R}^D$ denotes the feature extracted from the ith local region of the image $\mathbf{x}$ and $\boldsymbol{g}_k$ corresponds to the text prompt embedding for the kth class as defined in equation 2.

For any region i of the image $\mathbf{x}$, if it corresponds to the ID class, its ground-truth label y is expected to appear among the top-C predicted classes. Conversely, if the region is unrelated to any ID class (e.g., background noise), the true class is unlikely to rank within the top-C, due to the lack of strong semantic alignment. Leveraging this observation, one can define an index set $\mathcal{J}$ to identify such ID-irrelevant regions:

$$\mathcal{J} = \{i \in \mathcal{I} : \mathrm{rank}\left(\mathsf{Pr}_i(y \mid \mathbf{x})\right) > C\}. \tag{4}$$

Here, $\mathrm{rank}\left(\mathsf{Pr}_i(y \mid \mathbf{x})\right)$ denotes the rank of the true label y among the predicted scores over all ID classes and C is a hyperparameter or can be fixed based on prior knowledge about the number of fine-grained classes or semantic relationships in the dataset. The methods in (Miyai et al., 2023a; Yu et al., 2024; Xu et al., 2025) utilized such extracted ID-irrelevant features to increase the uncertainty of their softmax-based class probability predictions using an entropy regularization (ER) given by:

$$\mathcal{L}_{\mathrm{Ent}} = -\sum_{i \in \mathcal{J}} H\big(\boldsymbol{p}_i(\boldsymbol{x})\big), \tag{5}$$

where $H(\boldsymbol{p}) = -\sum_{k=1}^{K} p_k \log p_k$ denotes entropy function and $\boldsymbol{p}_i(\boldsymbol{x}),\ i \in \mathcal{J}$ is a K-dimensional probability vector, where each entry represents $\mathsf{Pr}_i(y = k \mid \boldsymbol{x})$, as defined in equation 3.

4 Proposed Approach

Motivation. The idea of using proxy OOD signals derived from ID-irrelevant regions in the training data is promising—especially since OOD data is typically unavailable at test time. Nonetheless, extracting more informative proxy OOD supervision is crucial as the budget of the training samples is limited under few-shot settings. Existing methods (Miyai et al., 2023a; Yu et al., 2024; Xu et al., 2025) rely on class prediction probabilities from ID/OOD regions to train the model to distinguish between ID and OOD data at test time. Yet, the high dimensional feature embeddings of the training data is much more informative—that is largely overlooked in the current approaches. In this context, a more robust and generalizable alternative would be to further incorporate the geometry of the feature representations captured by the rich representation power of the pretarined VLMs. This could make extraction of proxy-OOD supervision more effective in few-shot settings without incurring much computational overhead.

Our Idea: Prompt Vectors-induced Subspace Projection. To enhance the OOD detection on the prompt learning-based approaches, we propose to leverage subspace projection techniques on the extracted local regions of the training data. Prior work indicates that pretrained VLM embeddings (e.g., CLIP) for ID data exhibits *low-dimensionality* due to their class-informative nature (Zhu et al., 2023; Bhalla et al., 2024). We aim to exploit this geometry by learning a low-dimensional basis $\boldsymbol{W} \in \mathbb{R}^{D \times M}$ that spans the ID subspace. During optimization, we aim to increase the alignment of ID regions to the subspace spanned by $\boldsymbol{W}$ and

simultaneously inflate its orthogonal residual components for OOD regions. To this end, we parameterize the basis $\boldsymbol{W}$ with the same prompt vectors $\boldsymbol{\omega}_1, \ldots, \boldsymbol{\omega}_M$ used for context optimization, yielding a parameter-efficient design. In this way, the learned prompt vectors preserve the ID–OOD separating geometry of the feature space alongside the class-informative geometry induced by cosine similarity matching as defined in equation 2.

Consider the matrix formed by the prompt vectors $\boldsymbol{\omega}_1, \ldots, \boldsymbol{\omega}_M$, i.e., $\boldsymbol{W} = [\boldsymbol{\omega}_1, \boldsymbol{\omega}_2, \ldots, \boldsymbol{\omega}_M]$. We project the local feature vectors corresponding to ID data onto an M-dimensional subspace spanned by the column vectors of $\boldsymbol{W} \in \mathbb{R}^{D \times M}$, also called the ID subspace and denoted as $\mathcal{R}(\boldsymbol{W})$. At the same time, the features from ID-irrelevant or OOD regions are projected to lie in the null space $\mathcal{N}(\boldsymbol{W})$ orthogonal to $\mathcal{R}(\boldsymbol{W})$, defined as $\mathcal{N}(\boldsymbol{W}) = \left\{\boldsymbol{f} \in \mathbb{R}^D : \boldsymbol{W}^\top \boldsymbol{f} = \boldsymbol{0}\right\}$, which has dimension $D - M$. It is important to keep $M < D$, since when $M = D$, the null space becomes trivial (containing only the zero vector), thus limiting our ability to separate ID and OOD features effectively. This condition is typically satisfied in practice, as the number of prompt vectors M is usually small (e.g., $M \approx 16$ as suggested in (Zhou et al., 2022b; Miyai et al., 2023a)), whereas the dimensionality of CLIP embeddings is relatively large (e.g., $D = 512$). Based on these complementary projections, we propose *subspace regularizations* (SR) for the ID and OOD regions as follows:

$$\mathcal{L}_{\text{Sub-ID}} = \sum_{i \in \mathcal{J}'} \frac{\|\text{Proj}_{\boldsymbol{W}^\perp}(\boldsymbol{f}_i^{\text{in}}))\|_2}{\|\boldsymbol{f}_i^{\text{in}}\|_2}, \ \mathcal{L}_{\text{Sub-OOD}} = \sum_{i \in \mathcal{J}} \frac{\|\text{Proj}_{\boldsymbol{W}}(\boldsymbol{f}_i^{\text{in}})\|_2}{\|\boldsymbol{f}_i^{\text{in}}\|_2}, \tag{6}$$

where $\boldsymbol{f}_i^{\text{in}}$ denotes the ith local region feature for the data item $\mathbf{x}$, $\mathcal{J}'$ is the complement of the set $\mathcal{J}$, i.e., $\mathcal{J}' = \mathcal{I} \setminus \mathcal{J} = \{i \in \mathcal{I} \mid i \notin \mathcal{J}\}$, and the projections $\mathsf{Proj}_{\boldsymbol{W}^\perp}$ and $\mathsf{Proj}_{\boldsymbol{W}}$ are given by:

$$\mathsf{Proj}_{\boldsymbol{W}^\perp}(\boldsymbol{f}) = \left(\boldsymbol{I}_D - \boldsymbol{W}\left(\boldsymbol{W}^\top \boldsymbol{W}\right)^{-1} \boldsymbol{W}^\top\right) \boldsymbol{f}, \ \mathsf{Proj}_{\boldsymbol{W}}(\boldsymbol{f}) = \left(\boldsymbol{W}\left(\boldsymbol{W}^\top \boldsymbol{W}\right)^{-1} \boldsymbol{W}^\top\right) \boldsymbol{f}. \tag{7}$$

Here, the loss term $\mathcal{L}_{\text{Sub-ID}}$ encourages ID features to lie within the column space $\mathcal{R}(\boldsymbol{W})$ by minimizing their projected components in the orthogonal complement, $\mathcal{N}(\boldsymbol{W})$. Conversely, the loss term $\mathcal{L}_{\text{Sub-OOD}}$ promotes OOD features to lie in $\mathcal{N}(\boldsymbol{W})$ by suppressing their projections onto $\mathcal{R}(\boldsymbol{W})$.

Implementation. The proposed SRs in equation 6 can be easily integrated to the context optimization framework. As a result, we propose the following *geometry-aware prompt learning* criterion that combines the cross-entropy loss with the SRs as follows:

$$\mathcal{L} = (1 - \mathsf{Pr}(y|\boldsymbol{x})) \cdot \mathcal{L}_{\text{CE}} + \ \mathsf{Pr}(y|\boldsymbol{x}) \cdot (\lambda_1 \mathcal{L}_{\text{Sub-ID}} + \lambda_2 \mathcal{L}_{\text{Sub-OOD}} + \lambda_3 \mathcal{L}_{\text{Ent}}) \tag{8}$$

where $(\boldsymbol{x}, y)$ denotes the image-label pair of the ID data, $\mathcal{L}_{\text{CE}}$ is the cross-entropy loss as defined after equation 2, other regularization terms are defined in equation 6 and equation 5, and $\lambda_1, \lambda_2, \lambda_3 > 0$ are the respective regularization parameters. Here, we employ the modulation weights using the softmax probabilities $\mathsf{Pr}(y|\boldsymbol{x})$, as proposed in the recent work (Yu et al., 2024). This reweighting strategy enables dynamic adjustment of the classification and regularization loss contributions according to the model's confidence in its predictions. This implies that, when the model exhibits lower confidence, the contributions from both SR and ER losses are downweighted, as ID-irrelevant region selection in equation 4 becomes less reliable.

The final training loss averages $\mathcal{L}$ across all the training examples and can be easily learned using backpropagation-based optimizers in an end-to-end manner. We refer our approach (also see Fig. 1) as **Sub**space learning-based **Co**ntext **Op**timization (SubCoOp).

Remark 1 *As one can see, the SR computations do not introduce significant computational overhead, as the per-feature cost for the projection operation is $\mathcal{O}(dM + M^2)$, which is typically dominated by $\mathcal{O}(dM)$ since M is much smaller than the CLIP embedding dimension D. Consequently, this cost is negligible compared to the CLIP forward pass required to produce the feature embeddings. Moreover, to maintain $\boldsymbol{W}$ as a full-rank matrix with independent vectors representing the basis of the ID subspace, we could impose explicit orthogonality or full-rank regularizations (e.g., nuclear norm or log-determinant norm). However, in practice, a soft constraint using ℓ_2 regularization (weight decay) often suffices, as it encourages more uniform singular values across the M dimensions without introducing additional complex regularization terms, as*

Table 1: OOD detection performance of our method and the baselines on various OOD datasets. Here ID dataset is ImageNet-1k. All methods employ the same CLIP-ViT-B/16 backbone. Results with $\star$ marked are taken from (Miyai et al., 2023a; Yu et al., 2024).

Method	**iNaturalist**		**SUN**		**Places365**		**Textures**		**Average**	
	FPR95↓	AUROC↑	FPR95↓	AUROC↑	FPR95↓	AUROC↑	FPR95↓	AUROC↑	FPR95↓	AUROC↑
Zero-shot methods										
MCM*	30.94	94.61	37.67	92.56	44.76	89.76	57.91	86.10	42.82	90.76
GL-MCM*	15.18	96.71	30.42	93.09	38.85	89.90	57.93	83.63	35.47	90.83
Post-hoc methods with fine-tuned CLIP										
MSP*	74.57	77.74	76.95	73.97	79.72	72.18	73.66	74.84	74.98	76.22
ODIN*	98.93	57.73	88.72	78.42	87.80	76.88	85.47	71.49	90.23	71.13
EnergyScore*	64.98	87.18	46.42	91.17	57.40	87.33	50.39	88.22	54.80	88.48
ReAct*	65.57	86.87	46.17	91.04	56.85	87.42	49.88	88.13	54.62	88.37
MaxLogit*	60.88	88.03	44.83	91.16	55.54	87.45	48.72	88.63	52.49	88.82
Prompt tuning-based methods (16-shot)										
LSN	$46.40^{\pm 1.76}$	$91.91^{\pm 2.73}$	$31.86^{\pm 1.56}$	$93.21^{\pm 1.32}$	$40.61^{\pm 0.65}$	$90.05^{\pm 1.53}$	$47.21^{\pm 0.88}$	$88.98^{\pm 0.97}$	$41.52^{\pm 1.21}$	$91.04^{\pm 1.64}$
NegPrompt	$38.11^{\pm 1.15}$	$90.22^{\pm 0.78}$	$31.44^{\pm 0.29}$	$92.59^{\pm 0.18}$	$36.15^{\pm 2.05}$	$90.97^{\pm 0.78}$	$44.64^{\pm 1.34}$	$87.49^{\pm 0.52}$	$37.59^{\pm 1.21}$	$90.32^{\pm 0.57}$
IDLike	$9.71^{\pm 0.60}$	$98.05^{\pm 0.07}$	$38.93^{\pm 0.10}$	$90.54^{\pm 0.68}$	$47.06^{\pm 1.44}$	$88.06^{\pm 1.93}$	$32.82^{\pm 5.12}$	$91.89^{\pm 1.49}$	$32.12^{\pm 1.09}$	$92.14^{\pm 0.01}$
CoOp	$26.72^{\pm 2.09}$	$94.53^{\pm 0.36}$	$36.96^{\pm 0.87}$	$92.34^{\pm 0.15}$	$45.01^{\pm 1.45}$	$89.43^{\pm 0.15}$	$40.38^{\pm 1.45}$	$90.95^{\pm 0.18}$	$37.27^{\pm 1.47}$	$91.81^{\pm 0.21}$
LoCoOp	$18.70^{\pm 2.12}$	$96.09^{\pm 0.38}$	$22.83^{\pm 0.98}$	$95.12^{\pm 0.07}$	$34.78^{\pm 3.47}$	$91.52^{\pm 0.63}$	$43.75^{\pm 0.22}$	$89.81^{\pm 0.33}$	$30.02^{\pm 1.70}$	$93.14^{\pm 0.35}$
Local-Prompt	$9.16^{\pm 1.15}$	$98.01^{\pm 0.21}$	$24.03^{\pm 0.75}$	$94.71^{\pm 0.11}$	$32.82^{\pm 1.96}$	$92.32^{\pm 0.73}$	$46.58^{\pm 0.27}$	$88.95^{\pm 0.21}$	$28.15^{\pm 1.03}$	$93.50^{\pm 0.32}$
SCT	$16.14^{\pm 1.81}$	$96.68^{\pm 0.29}$	$21.57^{\pm 1.20}$	$95.23^{\pm 0.26}$	$31.47^{\pm 0.89}$	$91.89^{\pm 0.25}$	$43.75^{\pm 0.56}$	$88.83^{\pm 0.45}$	$28.23^{\pm 1.12}$	$93.16^{\pm 0.31}$
SubCoOp	$12.61^{\pm 1.69}$	$97.28^{\pm 0.38}$	$18.75^{\pm 1.47}$	$95.82^{\pm 0.20}$	$29.45^{\pm 1.66}$	$92.51^{\pm 0.13}$	$41.06^{\pm 1.02}$	$90.65^{\pm 0.25}$	$\mathbf{25.47}^{\pm \mathbf{1.46}}$	$\mathbf{94.07}^{\pm \mathbf{0.24}}$

Table 2: OOD detection performance of various prompt tuning-based approaches with and without subspace regularizations in 16-shot settings. Here ID dataset is ImageNet-1k dataset.

Method	**iNaturalist**		**SUN**		**Places365**		**Texture**		**Average**	
	FPR95↓	AUROC↑	FPR95↓	AUROC↑	FPR95↓	AUROC↑	FPR95↓	AUROC↑	FPR95↓	AUROC↑
CoOp	$14.70^{\pm 2.28}$	$96.40^{\pm 0.65}$	$28.07^{\pm 1.65}$	$92.60^{\pm 0.72}$	$37.37^{\pm 2.01}$	$89.78^{\pm 0.68}$	$43.55^{\pm 1.95}$	$87.55^{\pm 0.72}$	$30.92^{\pm 1.97}$	$91.58^{\pm 0.69}$
CoOp-SR	$14.85^{\pm 3.36}$	$96.76^{\pm 0.94}$	$25.19^{\pm 0.77}$	$94.62^{\pm 0.07}$	$33.34^{\pm 0.91}$	$91.24^{\pm 0.19}$	$41.85^{\pm 1.22}$	$89.74^{\pm 0.49}$	$\mathbf{28.81}^{\pm \mathbf{1.57}}$	$\mathbf{93.59}^{\pm \mathbf{0.42}}$
LoCoOp	$18.70^{\pm 2.12}$	$96.09^{\pm 0.38}$	$22.83^{\pm 0.98}$	$95.12^{\pm 0.07}$	$34.78^{\pm 3.47}$	$91.52^{\pm 0.63}$	$43.75^{\pm 0.22}$	$89.81^{\pm 0.33}$	$30.02^{\pm 1.70}$	$93.14^{\pm 0.35}$
LoCoOp-SR	$14.33^{\pm 0.76}$	$96.99^{\pm 0.08}$	$22.14^{\pm 1.96}$	$95.10^{\pm 0.44}$	$32.04^{\pm 2.82}$	$92.07^{\pm 0.61}$	$42.35^{\pm 3.04}$	$89.87^{\pm 0.53}$	$\mathbf{27.72}^{\pm \mathbf{2.15}}$	$\mathbf{93.51}^{\pm \mathbf{0.42}}$
SCT	$16.14^{\pm 1.81}$	$96.68^{\pm 0.29}$	$21.57^{\pm 1.20}$	$95.23^{\pm 0.26}$	$31.47^{\pm 0.89}$	$91.89^{\pm 0.25}$	$43.75^{\pm 0.56}$	$88.83^{\pm 0.45}$	$28.23^{\pm 1.12}$	$93.16^{\pm 0.31}$
SCT-SR	$12.61^{\pm 1.69}$	$97.28^{\pm 0.38}$	$18.75^{\pm 1.47}$	$95.82^{\pm 0.20}$	$29.45^{\pm 1.66}$	$92.51^{\pm 0.13}$	$41.06^{\pm 1.02}$	$90.65^{\pm 0.25}$	$\mathbf{25.47}^{\pm \mathbf{1.46}}$	$\mathbf{94.07}^{\pm \mathbf{0.24}}$
OSPCoOp	$14.28^{\pm 1.37}$	$97.11^{\pm 0.35}$	$18.95^{\pm 1.25}$	$96.52^{\pm 0.07}$	$27.18^{\pm 1.37}$	$93.52^{\pm 0.57}$	$41.75^{\pm 0.25}$	$90.96^{\pm 0.31}$	$25.54^{\pm 1.06}$	$94.53^{\pm 0.33}$
OSPCoOp-SR	$12.89^{\pm 1.73}$	$97..41^{\pm 0.41}$	$18.02^{\pm 1.36}$	$96.69^{\pm 0.12}$	$26.94^{\pm 1.22}$	$93.46^{\pm 0.52}$	$40.79^{\pm 0.22}$	$90.93^{\pm 0.35}$	$\mathbf{24.66}^{\pm \mathbf{1.13}}$	$\mathbf{94.62}^{\pm \mathbf{0.35}}$

shown in our experiments. Also, to ensure the matrix inversions in equation 7 is well-conditioned, we compute $(\boldsymbol{W}^\top \boldsymbol{W} + \epsilon I_M)^{-1}$*, where* $\epsilon > 0$ *is a small scalar that helps prevent rank deficiency and improve numerical stability.*

5 Experiments

In this section, we present extensive experiment results showcasing the effectiveness of our approach in few-shot OOD detection.

5.1 Setup

Dataset. We employ ImageNet-1k and ImageNet-100 datasets (Deng et al., 2009) as ID data. For OOD data, we use a number of commonly used benchmark datasets such as iNaturalist (Van Horn, 2018), SUN (Xiao et al., 2010), Places Zhou et al. (2017), and Texture (Van Horn et al., 2018). For the few-shot training, we use 1-16 images per ID class, and evaluate the model using the whole OOD datasets and the test ID dataset.

Implementation Details. We employ the ViT-B/16 model (Dosovitskiy et al., 2020) as the backbone of the

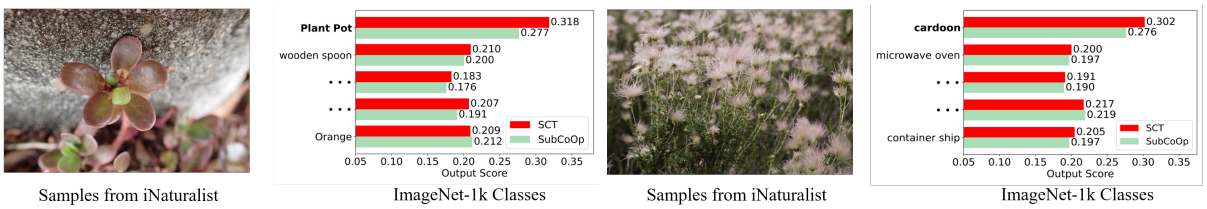

Samples from iNaturalist | ImageNet-1k Classes | Samples from iNaturalist | ImageNet-1k Classes

Figure 2: Example images from the iNaturalist dataset that are visually and semantically similar to certain ImageNet-1k classes. Comparison of similarity scores from SCT and our proposed SubCoOp. While SCT assigns high similarity scores to the ImageNet-1k ID classes, leading to incorrect detection as ID, SubCoOp effectively suppresses such scores, enabling the correct OOD detection.

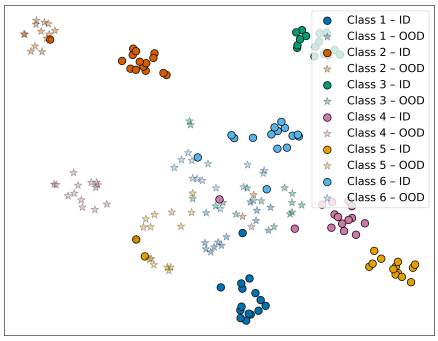

Figure 3: UMAP visualization of local ID and OOD local feature embeddings extracted by SubCoOp where we randomly choose 6 classes from the ImageNet-1K dataset for easier visualization.

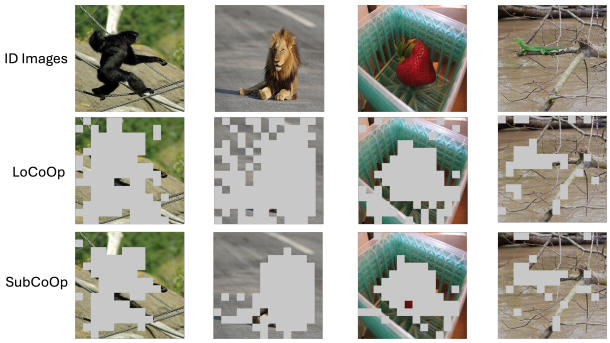

Figure 4: Visualization of extracted local ID (gray patches) and OOD regions (colored regions) with LoCoOp and SubCoOp method.

visual encoder for the pretrained CLIP model. For ID-irrelevant feature extraction, we set the rank threshold parameter C to the recommended value 100 and 20 for ImageNet-1k and ImageNet-100, respectively, based on the number of fine-grained classes (Miyai et al., 2023a). In addition, we fix $M = 16$, $\lambda_1 = 0.25$, $\lambda_2 = 2$, and $\lambda_3 = 5$, unless specified otherwise. We employ the SGD optimizer with a learning rate of 0.002, a batch size of 32, and train the model for 25 epochs. We use Nvidia 3090 Ti GPU for all the experiments.

OOD Detection Score: While testing, we adopt the global-local maximum concept matching (GL-MCM) score (Miyai et al., 2023b; 2025) for OOD detection (i.e., the score function $s(\mathbf{x})$ as employed in equation 1). This metric integrates the maximum softmax probability scores from both whole image feature and local image features and is defined as follows:

$$s_{\text{GL–MCM}}(\mathbf{x}) = \max_k \frac{\exp\left(\text{sim}(f, \mathbf{g}_k)/\tau\right)}{\sum_{k'=1}^{K} \exp\left(\text{sim}(f, \mathbf{g}_{k'})/\tau\right)} + \max_{k,i} \frac{\exp\left(\text{sim}(\boldsymbol{f}_i, \boldsymbol{g}_k)/\tau\right)}{\sum_{k'=1}^{K} \exp\left(\text{sim}(\boldsymbol{f}_i, \boldsymbol{g}_{k'})/\tau\right)} \tag{9}$$

where $\boldsymbol{f}$ is the vision encoder output for the test image $\mathbf{x}$, $\boldsymbol{f}_i$'s are its features corresponding to the local regions, and $\tau > 0$ denotes the temperature scaling parameter.

Evaluation Metrics. We evaluate the OOD detection performance using the following metrics: *(i)* FPR95 refers to the false positive rate (FPR) of OOD samples when the true positive rate (TPR) of ID samples is at 95%; *(ii)* area under the receiver operating characteristic curve (AUROC), measures the model's ability to distinguish between ID and OOD samples by evaluating TPR vs. FPR95 across all thresholds; and *(iii)* classification accuracy on ID data.

Baselines. To evaluate our proposed method, we consider a number of recently proposed prompt tuning-based approaches. Specifically, we employ LSN (Nie et al., 2024), NegPrompt (Liang et al., 2017), IDLike (Bai et al., 2024), CoOp (Zhou et al., 2022b), LoCoOp (Miyai et al., 2023a), and SCT (Yu et al., 2024). CoOp, LoCoOp, SCT and our approach SubCoOp are based on learning a set of positive prompts. On

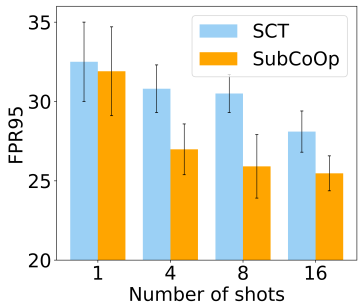

Figure 5: OOD detection performance of various few-shot techniques in ImageNet-1k dataset

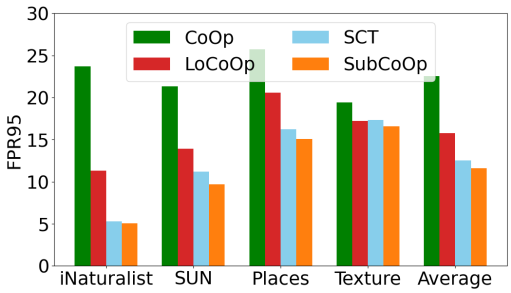

Figure 6: OOD performance of our method SubCoOp and other methods across various OOD datasets with ID dataset as ImageNet-100

Table 3: OOD detection performance comparison with LoCoOp on hard OOD detection tasks.

ID Dataset	OOD Dataset	Method	FPR95↓	AUROC↑
ImageNet-100	ImageNet-10	SCT	46.05	88.37
		SubCoOp	**44.34**	**88.58**
ImageNet-20	ImageNet-10	SCT	10.02	**97.96**
		SubCoOp	**9.15**	97.72
ImageNet-10	ImageNet-20	SCT	14.71	95.64
		SubCoOp	**12.63**	**95.92**
ImageNet-10	ImageNet-100	SCT	6.42	97.75
		SubCoOp	**5.92**	**97.95**
ImageNet-100	ImageNet-20	SCT	58.53	81.19
		SubCoOp	**57.17**	**81.34**

the other hand, NegPrompt and LSN each learn a set of negative prompts per ID class in addition to the positive prompt vectors. IDLike (Bai et al., 2024) is based on extracting outlier from ID data by performing spatial cropping on the images to enhance the OOD detection. In addition, we also compare with zero-shot approaches and post-hoc methods with CLIP fine tuning. For the zero shot baselines, we use the state-of-the-art MCM (Ming et al., 2022) and GL-MCM (Miyai et al., 2023b) methods. For the post-hoc methods, we adopt a number of popular OOD scoring methods such as MSP (Hendrycks & Gimpel, 2016), ReAcT (Sun et al., 2021), ODIN (Liang et al., 2017), MaxLogit Basart et al. (2022), and Energy Score (Liu et al., 2020b). These methods leverage CLIP's fine-tuned representations and combine them with simple post-processing techniques/scores for OOD detection. Unless otherwise specified, we adopt the same OOD detection score functions originally proposed by the respective methods. For instance, CoOp utilizes the MCM score, while both LoCoOp and SCT employ the GL-MCM score, similar to our approach SubCoOp. In addition, we include the recently proposed baseline OSPCoOp (Xu et al., 2025) in selected experiments, as its in-built segmentation-based inpainting makes it computationally expensive.

5.2 Main Results

SubCoOp's performance on ImageNet-1k. In Table 1, we present the OOD detection performance of our proposed approach and the baselines with ImageNet-1k as the ID dataset under different OOD datasets. The results are averaged over three random trials and the standard deviation is also reported. One can note that prompt tuning–based methods outperform other line of approaches as they encourage the model to align visual features with more discriminative and dynamically learned text prompts. More importantly, our proposed method SubCoOp outperforms the state-of-the-art prompt learning-based approaches with a notable margin. SubCoOp attains the best OOD detection performance, with a reduction of 2.76% in FPR95 and an improvement of 0.92% in AUROC compared to the next best performing method SCT. Our method particularly exhibit substantial improvements on challenging datasets such as iNaturalist and Places365, with an average FPR95 reduction of 3.53% and 2.82%, respectively compared to the SCT method. To provide a qualitative comparison, we present the class prediction probabilities output by SubCoOp, and by SCT on a

Table 4: OOD detection performance of SubCoOp under different SR and ER settings. ID dataset is ImageNet-1k. Here, × indicates a zero regularization parameter, and ✓ indicates a non-zero value.

λ_1	λ_2	λ_3	**iNaturalist**		**SUN**		**Places**		**Texture**		**Average**	
			FPR95↓	AUROC↑	FPR95↓	AUROC↑	FPR95↓	AUROC↑	FPR95↓	AUROC↑	FPR95↓	AUROC↑
×	×	×	$14.70^{\pm 2.28}$	$96.40^{\pm 0.65}$	$28.07^{\pm 1.65}$	$92.60^{\pm 0.72}$	$37.37^{\pm 2.01}$	$89.78^{\pm 0.68}$	$43.55^{\pm 1.95}$	$87.55^{\pm 0.72}$	$30.92^{\pm 1.97}$	$91.58^{\pm 0.69}$
×	×	✓	$16.14^{\pm 1.81}$	$96.68^{\pm 0.29}$	$21.57^{\pm 1.20}$	$95.23^{\pm 0.26}$	$31.47^{\pm 0.89}$	$91.89^{\pm 0.25}$	$43.75^{\pm 0.56}$	$88.83^{\pm 0.45}$	$28.23^{\pm 1.12}$	$93.16^{\pm 0.31}$
✓	×	✓	$14.12^{\pm 1.29}$	$97.61^{\pm 0.17}$	$20.62^{\pm 1.40}$	$95.77^{\pm 0.29}$	$30.16^{\pm 0.83}$	$92.42^{\pm 0.22}$	$42.64^{\pm 0.27}$	$89.15^{\pm 0.21}$	$26.89^{\pm 0.95}$	$93.74^{\pm 0.22}$
×	✓	✓	$15.45^{\pm 2.43}$	$96.89^{\pm 0.55}$	$20.52^{\pm 1.82}$	$95.61^{\pm 0.32}$	$30.12^{\pm 1.58}$	$92.48^{\pm 0.26}$	$43.21^{\pm 0.43}$	$88.82^{\pm 0.51}$	$27.33^{\pm 1.57}$	$93.45^{\pm 0.41}$
✓	✓	✓	$12.61^{\pm 1.69}$	$97.28^{\pm 0.38}$	$18.75^{\pm 1.47}$	$95.82^{\pm 0.20}$	$29.45^{\pm 1.66}$	$92.51^{\pm 0.13}$	$41.06^{\pm 1.02}$	$90.65^{\pm 0.25}$	$\mathbf{25.47^{\pm 1.46}}$	$\mathbf{94.07^{\pm 0.24}}$

Table 5: OOD performance of our method SubCoOp and other methods with OpenImage-O dataset as OOD and ImageNet-1k as ID

Method	FPR95↓	AUROC ↑
`SubCoOp`	**29.14**	**93.52**
`SCT`	32.62	92.78
`LoCoOp`	34.37	92.25
`CoOp`	35.85	91.92

few OOD samples from iNaturalist that is semantically similar to certain ID classes from ImageNet-1k, as shown in Fig. 2. SubCoOp also maintains high ID classification accuracy as shown in the supplementary material.

SR regularizations on other prompt tuning approaches. We further analyze the advantages of our proposed subspace regularizations (SR) by incorporating into other prompt-learning approaches. For example, the method CoOp (Zhou et al., 2022b) with SR is trained with the following modified objective function: $\mathcal{L}_{\text{CoOp-SR}} = \mathcal{L}_{\text{CE}} + \lambda_1 \mathcal{L}_{\text{Sub-ID}} + \lambda_2 \mathcal{L}_{\text{Sub-OOD}}$, where $\mathcal{L}_{\text{Sub-ID}}$ and $\mathcal{L}_{\text{Sub-OOD}}$ are defined in equation 6. Similarly, we can easily incorporate the proposed SR into other prompt learning-based approaches. In Table 2, we present the results that analyze the performance enhancement by the proposed subspace regularizations on various prompt learning techniques. For a fair comparison and to specifically highlight the contribution of the proposed SR, we employ the GL-MCM score for all the methods in Table 2. One can note that in all the cases, the proposed regularization improved the OOD performance by noticeable margin. For example, in the case of CoOp, CoOp-SR reduces the average FPR95 from 30.92% to 28.81% and boosts the average AUROC from 91.58% to 93.59%, with significant gains on the SUN and Places365 datasets. Similar performance gains are observed the case of LoCoOp method as well, further reinforcing the consistent performance enhancement by SR.

SubCoOp's performance across different few-shot settings. In Fig. 5, we compare the OOD detection performance of our method SubCoOp and the competing baseline SCT under varying few-shot settings with ImageNet-1k as the ID data set. Specifically, we present the average FPR95 and AUROC scores across all the OOD datasets under test. Both methods demonstrate consistent improvements in detection performance as the number of shots increases. Sub-CoOp generally outperforms SCT, particularly in the higher-shot settings, showing lower average FPR95 and higher average AUROC.

SubCoOp's performance on OpenImage-O dataset. Prior OOD datasets (e.g., Places, SUN) often contain samples that overlap with certain ID classes semantically or visually, which can lead to noisy and less reliable evaluations. OpenImage-O dataset Wang et al. (2022b) alleviates this issue through explicit image-level validation and more reliable OOD benchmarking. We additionally report OOD detection performance on the OpenImage-O dataset in Table 5. Here, ImageNet-1K is treated as the ID dataset, while OpenImage-O serves as the OOD dataset.

SubCoOp's performance on ImageNet-100. Fig. 6 presents the OOD detection performance of various prompt learning methods under the 16-shot setting, using ImageNet-100 as the ID dataset. SubCoOp

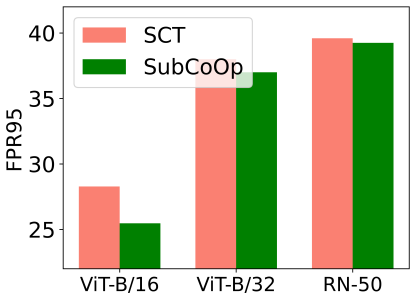

Figure 7: Average OOD detection performance across different image encoders for ImageNet-1k dataset

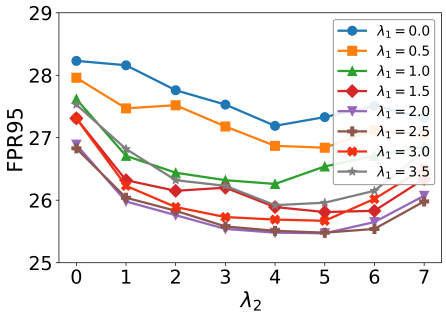

Figure 8: Average OOD detection performance of SubCoOp across different values of λ_1 and λ_2 using ImageNet-1k as the ID dataset.

outperforms all baselines under test, achieving the lowest average FPR95 (11.60%) and the highest average AUROC (97.80%). Compared to SCT and LoCoOp, SubCoOp demonstrates consistent detection performance across all OOD datasets. More results and discussion related to ImageNet-100 are relegated to supplementary section.

Visualization of ID-OOD feature geometry in SubCoOp. Figure 3 visualizes the UMAP projection of local feature embeddings extracted by SubCoOp from both ID-relevant and ID-irrelevant (proxy OOD) regions. We observe that ID-relevant features form compact and well-separated class clusters, whereas the ID-irrelevant features are distributed farther from their corresponding class centers and exhibit reduced overlap with ID clusters. This highlights SubCoOp's effectiveness in promoting a discriminative subspace for ID/OOD separation. This geometry, which was not exploited in prior approaches like LoCoOp and SCT, leads to better ID and OOD local region extraction for SubCoOp. Figure 4 compares the ID/OOD local region extraction selected by LoCoOp and our SubCoOp. The top row shows the original ID images, while the middle and bottom rows correspond to LoCoOp and SubCoOp, respectively. SubCoOp applies subspace regularization to explicitly disentangle ID-relevant and ID-irrelevant features, yielding more coherent and semantically meaningful OOD regions. This results in cleaner ID/OOD separation both visually and quantitatively.

SubCoOp's performance on hard OOD detection tasks. Table 3 presents the hard OOD detection results of our SubCoOp method across multiple ID–OOD dataset pairs. One can note that SubCoOp consistently outperforms the competing baseline SCT in all four cases, highlighting its robustness against semantically hard OOD data.

5.3 Ablation Studies

Performance enhancement by SR. As discussed, the critical component of our proposed approach is the subspace regularizations (SR) as defined in equation 6. In this section, we analyze the contribution of each component of the SR in enhancing the OOD detection performance. Table 4 shows that removing both the ID and OOD regularization terms (i.e., setting $\lambda_1 = 0$, $\lambda_2 = 0$) leads to the lowest detection performance among all tested scenarios. Introducing only the ID subspace regularization (i.e., $\lambda_1 \neq 0$, $\lambda_2 = 0$) yields substantial performance improvement, as projecting ID-relevant features onto the subspace spanned by the prompt vectors enhances the desired ID-OOD separability during inference. On the other hand, applying only the OOD subspace regularization provides limited performance gain, as expected. The best results are obtained when both regularization terms are used jointly, underscoring the effectiveness of simultaneously projecting ID features onto the column space and OOD features onto the orthogonal null space.

Different image encoders. We evaluate our proposed SubCoOp method across different image encoder architectures for CLIP, with results summarized in Fig. 7. The results show that SubCoOp consistently outperforms SCT across ViT-B/16, ViT-B/32 and ResNet (RN)-50 backbones and observed to be particularly

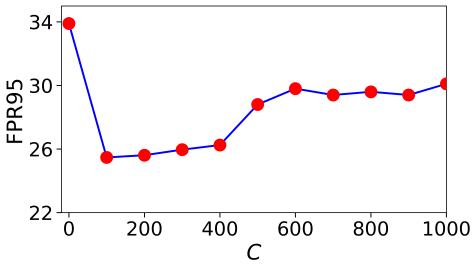

Figure 9: Average OOD detection performance of SubCoOp across different values of C using ImageNet-1k dataset.

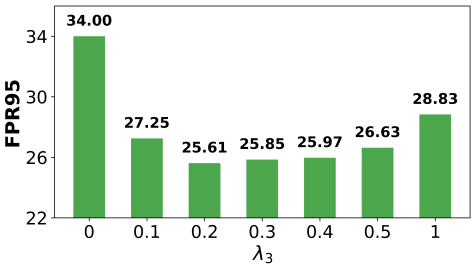

Figure 10: Average OOD detection performance of SubCoOp across different values of ER regularizer λ_3 using ImageNet-1k dataset.

effective in transformer-based models. SubCoOp achieved the best performance using the ViT-B/16 architecture. With ViT-B/32 as well, SubCoOp outperforms SCT by reducing the average FPR95 by 0.92% and increasing AUROC by 0.56%. For ResNet-50 architecture, SubCoOp maintains competitive OOD detection performance.

Varying SR hyperparameters. We analyze the impact of varying ID SR hyperparameter λ_1 and OOD SR hyperparameter λ_2 (see equation 8) on the performance of our SubCoOp method, as shown in Fig. 8. In general, $\lambda_1 = 2$ achieves the lowest FPR95 and AUROC in ImageNet-1k, while maintaining more or less consistent performance across different λ_2 values. As one can observe, our method is more sensitive to ID SR regularizer λ_1. Both excessively high and low values of λ_1 degrade OOD detection performance. When λ_1 is small, the regularizer has minimal influence, resulting in unstructured latent features. In contrast, excessive regularization constrains the latent representations too tightly to a learned subspace, potentially suppressing certain discriminative features that are crucial for distinguishing ID from OOD samples. Hence, selecting an appropriate value for λ_1 is crucial for our approach. As shown in Fig. 8, the configuration $\lambda_1 = 2, \lambda_2 = 5$ achieves the best overall performance, resulting an FPR95 of 25.47% and an AUROC of 94.07%.

Varying ER hyperparameter λ_3 and rank threshold C. Fig. 9 and 10 analyzes the impact of varying C values and ER hyperparameter λ_3, respectively, for our SubCoOp approach. We evaluate C values ranging from 0 to 1,000 under the 16-shot setting. SubCoOp exhibits degraded performance at $C = 0$, where all local regions are treated as OOD, leading to high false positive rates. In Fig. 9, as C increases, particularly in the range of between 100 and 400, FPR95 decreases and AUROC improves, indicating more accurate selection of OOD-relevant local features. In Fig. 10, as the regularization parameter λ_3 increases from 0, SubCoOp shows performance improvement with a notable decrease in FPR95 and an increase in AUROC, achieving peak performance around weight 0.2. Beyond a weight of 0.3, SubCoOp's performance slightly deteriorates, suggesting that overly strong ER regularization may hinder detection.

More experiment results, ablation studies, implementation settings, and related discussions are presented in supplementary section.

6 Conclusion

In this work, we propose a novel approach that integrates subspace representation learning with prompt optimization in VLMs for few-shot OOD detection. Our method induces a distinctive geometry in the feature embedding space by projecting ID features onto a subspace spanned by learnable prompt vectors, while pushing ID-irrelevant features to the orthogonal null space. Experiments on several OOD benchmarks based on ImageNet-1k and ImageNet-100 demonstrate that our prompt tuning framework, SubCoOp, consistently outperforms state-of-the-art methods in OOD detection, without sacrificing ID classification accuracy.

References

Yichen Bai, Zongbo Han, Bing Cao, Xiaoheng Jiang, Qinghua Hu, and Changqing Zhang. Id-like prompt learning for few-shot out-of-distribution detection. In *Proceedings of the IEEE/CVF Conference on Computer Vision and Pattern Recognition*, pp. 17480–17489, 2024.

Steven Basart, Mazeika Mantas, Mostajabi Mohammadreza, Steinhardt Jacob, and Song Dawn. Scaling out-of-distribution detection for real-world settings. In *International Conference on Machine Learning*, 2022.

Usha Bhalla, Alex Oesterling, Suraj Srinivas, Flavio Calmon, and Himabindu Lakkaraju. Interpreting clip with sparse linear concept embeddings (splice). *Advances in Neural Information Processing Systems*, 37: 84298–84328, 2024.

Chentao Cao, Zhun Zhong, Zhanke Zhou, Yang Liu, Tongliang Liu, and Bo Han. Envisioning outlier exposure by large language models for out-of-distribution detection. *arXiv preprint arXiv:2406.00806*, 2024.

Jia Deng, Wei Dong, Richard Socher, Li-Jia Li, Kai Li, and Li Fei-Fei. Imagenet: A large-scale hierarchical image database. In *2009 IEEE Conference on Computer Vision and Pattern Recognition*, pp. 248–255, 2009. doi: 10.1109/CVPR.2009.5206848.

Taylor Denouden, Rick Salay, Krzysztof Czarnecki, Vahdat Abdelzad, Buu Phan, and Sachin Vernekar. Improving reconstruction autoencoder out-of-distribution detection with mahalanobis distance. *arXiv preprint arXiv:1812.02765*, 2018.

Choubo Ding and Guansong Pang. Zero-shot out-of-distribution detection with outlier label exposure. In *2024 International Joint Conference on Neural Networks (IJCNN)*, pp. 1–8. IEEE, 2024.

Alexey Dosovitskiy, Lucas Beyer, Alexander Kolesnikov, Dirk Weissenborn, Xiaohua Zhai, Thomas Unterthiner, Mostafa Dehghani, Matthias Minderer, Georg Heigold, Sylvain Gelly, et al. An image is worth 16x16 words: Transformers for image recognition at scale. *arXiv preprint arXiv:2010.11929*, 2020.

Sepideh Esmaeilpour, Bing Liu, Eric Robertson, and Lei Shu. Zero-shot out-of-distribution detection based on the pre-trained model clip. In *Proceedings of the AAAI conference on artificial intelligence*, volume 36, pp. 6568–6576, 2022.

Xiang Fang, Arvind Easwaran, and Blaise Genest. Adaptive multi-prompt contrastive network for few-shot out-of-distribution detection. *arXiv preprint arXiv:2506.17633*, 2025.

Christiane Fellbaum. Wordnet. In *Theory and applications of ontology: computer applications*, pp. 231–243. Springer, 2010.

Hao Fu, Naman Patel, Prashanth Krishnamurthy, and Farshad Khorrami. Clipscope: Enhancing zero-shot ood detection with bayesian scoring. In *2025 IEEE/CVF Winter Conference on Applications of Computer Vision (WACV)*, pp. 5346–5355. IEEE, 2025.

Andreas Geiger, Philip Lenz, and Raquel Urtasun. Are we ready for autonomous driving? the kitti vision benchmark suite. In *2012 IEEE conference on computer vision and pattern recognition*, pp. 3354–3361. IEEE, 2012.

Ian J Goodfellow, Jonathon Shlens, and Christian Szegedy. Explaining and harnessing adversarial examples. *arXiv preprint arXiv:1412.6572*, 2014.

Dan Hendrycks and Kevin Gimpel. A baseline for detecting misclassified and out-of-distribution examples in neural networks. *arXiv preprint arXiv:1610.02136*, 2016.

Dan Hendrycks, Steven Basart, Mantas Mazeika, Andy Zou, Joseph Kwon, Mohammadreza Mostajabi, Jacob Steinhardt, and Dawn Song. Scaling out-of-distribution detection for real-world settings. In *Proceedings of the 39th International Conference on Machine Learning (ICML)*, pp. 8759–8773. PMLR, 2022. URL `https://proceedings.mlr.press/v162/hendrycks22a.html`.

Rui Huang and Yixuan Li. Mos: Towards scaling out-of-distribution detection for large semantic space. In *Proceedings of the IEEE/CVF Conference on Computer Vision and Pattern Recognition*, pp. 8710–8719, 2021.

Rui Huang, Andrew Geng, and Yixuan Li. On the importance of gradients for detecting distributional shifts in the wild. *Advances in Neural Information Processing Systems*, 34:677–689, 2021.

Menglin Jia, Luming Tang, Bor-Chun Chen, Claire Cardie, Serge Belongie, Bharath Hariharan, and Ser-Nam Lim. Visual prompt tuning. In *European conference on computer vision*, pp. 709–727. Springer, 2022.

Xue Jiang, Feng Liu, Zhen Fang, Hong Chen, Tongliang Liu, Feng Zheng, and Bo Han. Negative label guided ood detection with pretrained vision-language models. *arXiv preprint arXiv:2403.20078*, 2024.

Polina Kirichenko, Pavel Izmailov, and Andrew G Wilson. Why normalizing flows fail to detect out-of-distribution data. *Advances in neural information processing systems*, 33:20578–20589, 2020.

Kimin Lee, Kibok Lee, Honglak Lee, and Jinwoo Shin. A simple unified framework for detecting out-of-distribution samples and adversarial attacks. *Advances in neural information processing systems*, 31, 2018.

Tianqi Li, Guansong Pang, Xiao Bai, Wenjun Miao, and Jin Zheng. Learning transferable negative prompts for out-of-distribution detection. In *CVPR*, 2024.

Shiyu Liang, Yixuan Li, and Rayadurgam Srikant. Enhancing the reliability of out-of-distribution image detection in neural networks. *arXiv preprint arXiv:1706.02690*, 2017.

Weitang Liu, Xiaoyun Wang, John Owens, and Yixuan Li. Energy-based out-of-distribution detection. *Advances in neural information processing systems*, 33:21464–21475, 2020a.

Weitang Liu, Xiaoyun Wang, John Douglas Owens, and Yixuan Li. Energy-based out-of-distribution detection. *ArXiv*, abs/2010.03759, 2020b. URL `https://api.semanticscholar.org/CorpusID:222208700`.

Xixi Liu and Christopher Zach. Tag: Text prompt augmentation for zero-shot out-of-distribution detection supplementary material. ECCV, 2024.

Xixi Liu, Yaroslava Lochman, and Christopher Zach. Gen: Pushing the limits of softmax-based out-of-distribution detection. In *Proceedings of the IEEE/CVF conference on computer vision and pattern recognition*, pp. 23946–23955, 2023.

Yifei Ming, Ziyang Cai, Jiuxiang Gu, Yiyou Sun, Wei Li, and Yixuan Li. Delving into out-of-distribution detection with vision-language representations. *Advances in neural information processing systems*, 35: 35087–35102, 2022.

Atsuyuki Miyai, Qing Yu, Go Irie, and Kiyoharu Aizawa. Locoop: Few-shot out-of-distribution detection via prompt learning. *Advances in Neural Information Processing Systems*, 36:76298–76310, 2023a.

Atsuyuki Miyai, Qing Yu, Go Irie, and Kiyoharu Aizawa. Zero-shot in-distribution detection in multi-object settings using vision-language foundation models. *arXiv preprint arXiv:2304.04521*, 2023b.

Atsuyuki Miyai, Qing Yu, Go Irie, and Kiyoharu Aizawa. Gl-mcm: Global and local maximum concept matching for zero-shot out-of-distribution detection. *International Journal of Computer Vision*, pp. 1–11, 2025.

Jun Nie, Yonggang Zhang, Zhen Fang, Tongliang Liu, Bo Han, and Xinmei Tian. Out-of-distribution detection with negative prompts. In *The twelfth international conference on learning representations*, 2024.

Jaewoo Park, Jacky Chen Long Chai, Jaeho Yoon, and Andrew Beng Jin Teoh. Understanding the feature norm for out-of-distribution detection. In *Proceedings of the IEEE/CVF international conference on computer vision*, pp. 1557–1567, 2023a.

Jaewoo Park, Yoon Gyo Jung, and Andrew Beng Jin Teoh. Nearest neighbor guidance for out-of-distribution detection. In *Proceedings of the IEEE/CVF international conference on computer vision*, pp. 1686–1695, 2023b.

Fabio Petroni, Tim Rocktäschel, Patrick Lewis, Anton Bakhtin, Yuxiang Wu, Alexander H Miller, and Sebastian Riedel. Language models as knowledge bases? *arXiv preprint arXiv:1909.01066*, 2019.

Alec Radford, Jong Wook Kim, Chris Hallacy, Aditya Ramesh, Gabriel Goh, Sandhini Agarwal, Girish Sastry, Amanda Askell, Pamela Mishkin, Jack Clark, et al. Learning transferable visual models from natural language supervision. In *International conference on machine learning*, pp. 8748–8763. PmLR, 2021.

Kuniaki Saito, Donghyun Kim, Stan Sclaroff, and Kate Saenko. Universal domain adaptation through self supervision. *Advances in neural information processing systems*, 33:16282–16292, 2020.

Thomas Schlegl, Philipp Seeböck, Sebastian M. Waldstein, Ursula Schmidt-Erfurth, and Georg Langs. Unsupervised anomaly detection with generative adversarial networks to guide marker discovery. In *Information Processing in Medical Imaging*, pp. 146–157. Springer International Publishing, 2017.

Vikash Sehwag, Mung Chiang, and Prateek Mittal. Ssd: A unified framework for self-supervised outlier detection. *arXiv preprint arXiv:2103.12051*, 2021.

Xu Shen, Yili Wang, Kaixiong Zhou, Shirui Pan, and Xin Wang. Optimizing ood detection in molecular graphs: A novel approach with diffusion models. In *Proceedings of the 30th ACM SIGKDD Conference on Knowledge Discovery and Data Mining*, pp. 2640–2650, 2024.

Yiyou Sun, Chuan Guo, and Yixuan Li. React: Out-of-distribution detection with rectified activations. *Advances in neural information processing systems*, 34:144–157, 2021.

Jihoon Tack, Sangwoo Mo, Jongheon Jeong, and Jinwoo Shin. Csi: Novelty detection via contrastive learning on distributionally shifted instances. In *Advances in Neural Information Processing Systems (NeurIPS)*, 2020.

Grant Van Horn. Oisin mac aodha, yang song, yin cui, chen sun, alex shepard, hartwig adam, pietro perona, and serge belongie. the inaturalist species classification and detection dataset. In *Proceedings of the IEEE conference on computer vision and pattern recognition*, volume 2, pp. 5, 2018.

Grant Van Horn, Oisin Mac Aodha, Yang Song, Yin Cui, Chen Sun, Alex Shepard, Hartwig Adam, Pietro Perona, and Serge Belongie. The inaturalist species classification and detection dataset. In *Proceedings of the IEEE conference on computer vision and pattern recognition*, pp. 8769–8778, 2018.

Haoqi Wang, Zhizhong Li, Litong Feng, and Wayne Zhang. Vim: Out-of-distribution with virtual-logit matching. In *Proceedings of the IEEE/CVF Conference on Computer Vision and Pattern Recognition (CVPR)*, pp. 4921–4930, June 2022a.

Haoqi Wang, Zhizhong Li, Litong Feng, and Wayne Zhang. Vim: Out-of-distribution with virtual-logit matching. In *Proceedings of the IEEE/CVF conference on computer vision and pattern recognition*, pp. 4921–4930, 2022b.

Hualiang Wang, Yi Li, Huifeng Yao, and Xiaomeng Li. Clipn for zero-shot ood detection: Teaching clip to say no. In *Proceedings of the IEEE/CVF International Conference on Computer Vision*, pp. 1802–1812, 2023.

Jianxiong Xiao, James Hays, Krista A Ehinger, Aude Oliva, and Antonio Torralba. Sun database: Large-scale scene recognition from abbey to zoo. In *2010 IEEE computer society conference on computer vision and pattern recognition*, pp. 3485–3492. IEEE, 2010.

Zhuo Xu, Xiang Xiang, and Yifan Liang. Overcoming shortcut problem in vlm for robust out-of-distribution detection. In *Proceedings of the Computer Vision and Pattern Recognition Conference*, pp. 15402–15412, 2025.

Jingkang Yang, Kaiyang Zhou, Yixuan Li, and Ziwei Liu. Generalized out-of-distribution detection: A survey. *International Journal of Computer Vision*, 132(12):5635–5662, 2024a.

Ying Yang, De Cheng, Chaowei Fang, Yubiao Wang, Changzhe Jiao, Lechao Cheng, Nannan Wang, and Xinbo Gao. Diffusion-based layer-wise semantic reconstruction for unsupervised out-of-distribution detection. *Advances in Neural Information Processing Systems*, 37:26846–26871, 2024b.

Geng Yu, Jianing Zhu, Jiangchao Yao, and Bo Han. Self-calibrated tuning of vision-language models for out-of-distribution detection. In *NeurIPS*, 2024.

Mert Yuksekgonul, Federico Bianchi, Pratyusha Kalluri, Dan Jurafsky, and James Zou. When and why vision-language models behave like bags-of-words, and what to do about it? *arXiv preprint arXiv:2210.01936*, 2022.

Fanhu Zeng, Zhen Cheng, Fei Zhu, Hongxin Wei, and Xu-Yao Zhang. Local-prompt: Extensible local prompts for few-shot out-of-distribution detection. *arXiv preprint arXiv:2409.04796*, 2024.

Yabin Zhang, Wenjie Zhu, Chenhang He, and Lei Zhang. Lapt: Label-driven automated prompt tuning for ood detection with vision-language models. In *European conference on computer vision*, pp. 271–288. Springer, 2024a.

Zihan Zhang, Zhuo Xu, and Xiang Xiang. Vision-language dual-pattern matching for out-of-distribution detection. In *European Conference on Computer Vision*, pp. 273–291. Springer, 2024b.

Bolei Zhou, Agata Lapedriza, Aditya Khosla, Aude Oliva, and Antonio Torralba. Places: A 10 million image database for scene recognition. *IEEE transactions on pattern analysis and machine intelligence*, 40(6): 1452–1464, 2017.

Kaiyang Zhou, Jingkang Yang, Chen Change Loy, and Ziwei Liu. Conditional prompt learning for vision-language models. In *Proceedings of the IEEE/CVF conference on computer vision and pattern recognition*, pp. 16816–16825, 2022a.

Kaiyang Zhou, Jingkang Yang, Chen Change Loy, and Ziwei Liu. Learning to prompt for vision-language models. *International Journal of Computer Vision*, 130(9):2337–2348, 2022b.

Xiangyang Zhu, Renrui Zhang, Bowei He, Aojun Zhou, Dong Wang, Bin Zhao, and Peng Gao. Not all features matter: Enhancing few-shot clip with adaptive prior refinement. In *Proceedings of the IEEE/CVF international conference on computer vision*, pp. 2605–2615, 2023.

Supplementary Material of "Prompt Optimization Meets Subspace Representation Learning for Few-shot Out-of-Distribution Detection"

A Related Works

OOD Detection. Traditional approaches to OOD detection can be broadly categorized into logit-based (Liu et al., 2020b; Hendrycks et al., 2022; Sun et al., 2021), feature-based (Lee et al., 2018; Saito et al., 2020; Park et al., 2023a), probability-based (Sun et al., 2021; Basart et al., 2022; Liang et al., 2017; Huang et al., 2021), and reconstruction-based methods (Yang et al., 2024b). Feature-based methods extract intermediate representations from ID data using a discriminative model and measure distances, such as the Mahalanobis distance, between test samples and the ID feature distribution (Denouden et al., 2018). Recent variants improve robustness by leveraging self-supervised or pre-trained models for more discriminative features (Tack et al., 2020; Sehwag et al., 2021). Recently ViM (Wang et al., 2022a) introduces a virtual OOD logit by projecting features onto a residual space and matching it with class logits to compute a robust joint OOD confidence score. GEN (Liu et al., 2023) uses a generalized entropy score computed from the output softmax score, amplifying small deviations from one-hot predictions to separate ID and OOD samples. NNGuide (Park et al., 2023b) uses nearest-neighbor feature similarity to guide confidence and reduce overconfidence on OOD samples.

Training-Free OOD Detection with Vision-Language Models. The advent of vision-language models, particularly CLIP (Radford et al., 2021), has opened new research frontiers for training-free OOD detection by leveraging powerful pre-trained joint representations. These methods utilize scoring functions to quantify the semantic discrepancy between ID and OOD samples without requiring model fine-tuning. Early works such as ZOC (Esmaeilpour et al., 2022), and MCM (Ming et al., 2022) apply CLIP-based embeddings for OOD detection using similarity-based metrics. GL-MCM (Miyai et al., 2025) extends this MCM score by incorporating local visual features to enhance OOD detection performance. CLIPN (Wang et al., 2023) proposes negative text encoders to better seperate OOD samples. DPM (Zhang et al., 2024b) matches domain-specific visual features with both textual and visual prototypes, improving ID–OOD separability. TAG (Liu & Zach, 2024) introduces text prompt augmentation strategy to increase the seperation between ID and OOD samples without requiring prompt optimization. In addition, outlier exposure methods like NegLabel (Jiang et al., 2024) leverages a large set of semantically diverse negative labels from WordNet (Fellbaum, 2010) to enhance separability between ID and OOD samples. LAPT (Zhang et al., 2024a) utlilizes large text corpora as external knowledge to mine negative label automatically and optimize distribution-aware prompts. CLIP-Scope (Fu et al., 2025) mines nearest and farthest WordNet (Fellbaum, 2010) labels for broad OOD coverage and applies a Bayesian posterior update using historical class-likelihoods to enhance zero-shot OOD detection. Meanwhile, OLE (Ding & Pang, 2024) explore synthetic outlier generation and EOE (Cao et al., 2024) utilizes expert-guided knowledge to improve OOD detection task.

Prompt Learning for OOD Detection. Prompt learning has recently emerged as an effective and parameter-efficient paradigm for adapting foundation models to novel tasks under limited supervision. Initially introduced in NLP (Petroni et al., 2019), prompt tuning utlilizes trainable prompt tokens to the input rather than updating the full model. In the vision-language domain, CoOp (Zhou et al., 2022b) proposes learning a set of shared context tokens, while CoCoOp (Zhou et al., 2022a) improves adaptability by making prompts conditional on the visual input features. VPT (Jia et al., 2022) further extends this approach by injecting prompts into the visual encoder layers. While this approaches are effective for in-distribution classification, they often struggle in OOD settings, as prompt tuning methods usually optimize for ID accuracy without explicitly addressing semantic shifts in OOD inputs. To address this, LoCoOp (Miyai et al., 2023a) regularizes prompt learning using CLIP's local features as surrogate OOD features. Similarly, LSN (Nie et al., 2024) and NegPrompt (Li et al., 2024) incorporate negative prompts to enhance the semantic separation between ID and OOD categories. ID-Like Bai et al. (2024) constructs challenging OOD samples by cropping ID images in the vicinity space and selecting low-similarity regions using CLIP.

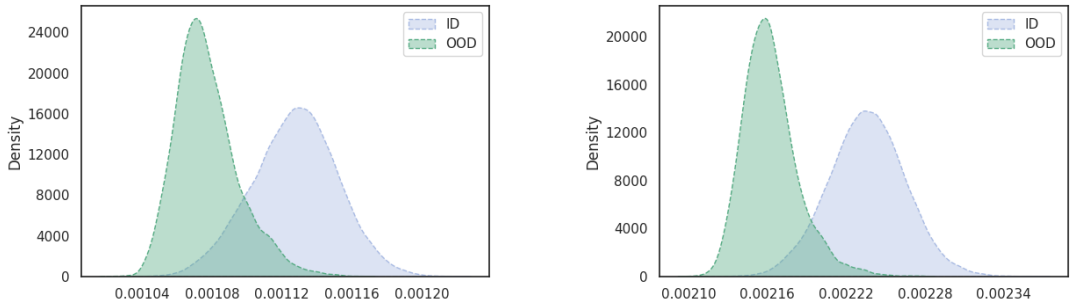

(a) (b)

Figure 11: OOD detection performance on the iNaturalist dataset using (a) SCT and (b) SubCoOp (Ours).

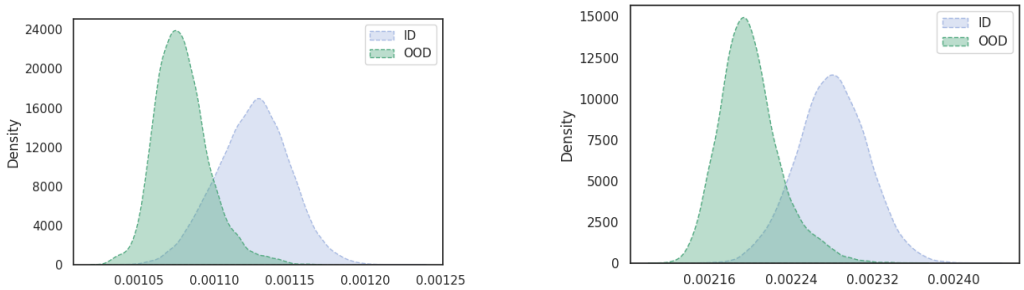

(a) (b)

Figure 12: OOD detection performance on the SUN dataset using (a) SCT and (b) SubCoOp (Ours).

B Additional Experiments

Figures 11 and 12 show ID/OOD histograms for iNaturalist and SUN, comparing SCT with SubCoOp. SubCoOp provides better separation between ID and OOD distributions, with reduced overlap in plots (b), highlighting its stronger capability to discriminate OOD samples. This minimal overlap between ID and OOD distributions demonstrates the strong separability achieved by our subspace regularization.

Table 10 compares the OOD detection performance of SCT and SubCoOp under varying few-shot settings using ImageNet-1k as the ID data set. Both methods demonstrate consistent improvements in FPR95 and AUROC as the number of shots increases. SubCoOp demonstrates a substantial performance gain over SCT, especially in higher-shot settings, achieving lower average FPR95 and higher average AUROC. In the 8-shot setting, SubCoOp consistently outperforms SCT across all OOD datasets, reducing average FPR95 from 30.57% to 26.11% and improving AUROC from 92.94% to 93.49%. Notable gains include substantial FPR95 reductions on SUN of 5.76% and Texture of 7.35%, highlighting SubCoOp's superior OOD separability when more labeled examples are available.

Table 6 presents OOD detection results across four OOD datasets for two backbone architectures, ViT-B/32 and RN-50, comparing SCT with SubCoOp. We present the ID classification performance of different methods in Table 7. Zero-shot and post-hoc methods achieve 66.7% ID accuracy on ImageNet-1k, whereas prompt-tuning approaches such as CoOp and NegPrompt improve this to approximately 71.92%. On the other hand, IDLike and LoCoOp attain 71.04% and 71.43% ID accuracy, respectively. Our proposed SubCoOp achieves a comparable 70.57% ID accuracy while delivering the best overall OOD detection performance.

Table 8 presents the effect of varying the entropy regularization weight (λ_3) on OOD detection performance for SubCoOp. It is evident that moderate values of λ_3 between 0.2 and 0.3 consistently obtain the best trade-off between FPR95 and AUROC across all four OOD datasets. For instance, λ_3=0.2 achieves the lowest average FPR95 of 25.64% with a corresponding AUROC of 94.02%, while λ_3=0.3 delivers a comparable

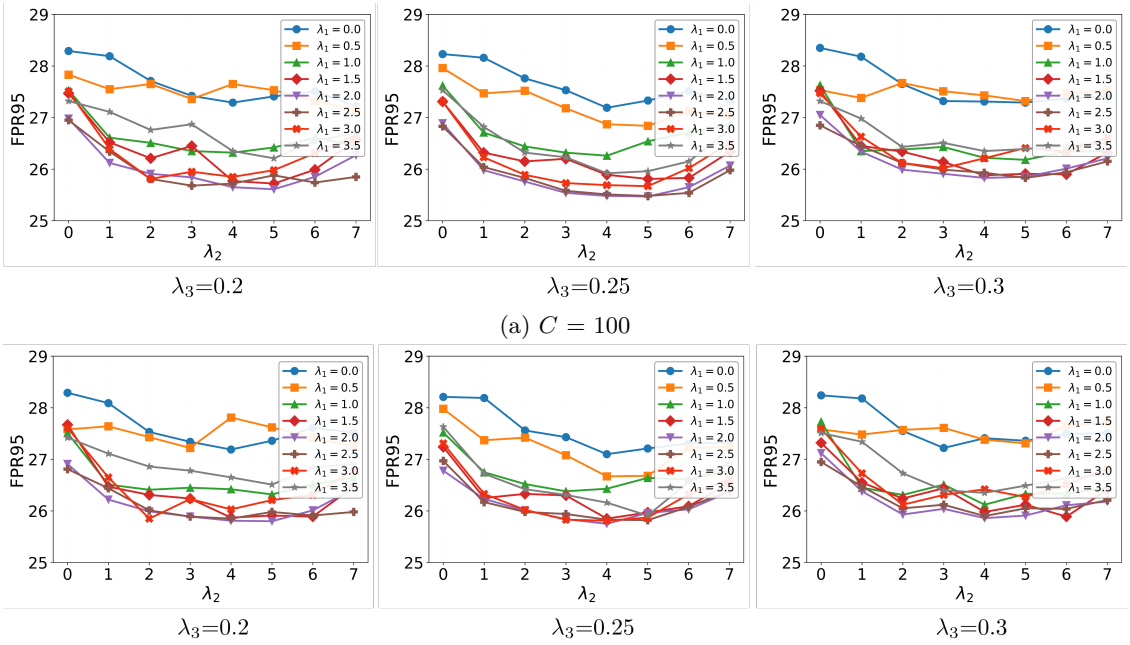

λ_3=0.2 λ_3=0.25 λ_3=0.3

(a) $C = 100$

λ_3=0.2 λ_3=0.25 λ_3=0.3

(b) $C = 200$

Figure 13: Performance analysis of our proposed SubCoOp method across different hyperparameters using ImageNet-1k dataset.

Table 6: OOD detection performance analysis with different backbones with ImageNet-1k dataset.

Model	Method	iNaturalist		SUN		Places		Texture		Avg	
		FPR95↓	AUROC↑	FPR95↓	AUROC↑	FPR95↓	AUROC↑	FPR95↓	AUROC↑	FPR95↓	AUROC↑
ViT-B/32	SCT	$29.07^{\pm 3.90}$	$94.24^{\pm 0.44}$	$35.27^{\pm 2.87}$	$92.47^{\pm 0.40}$	$39.59^{\pm 2.40}$	$90.36^{\pm 0.42}$	$47.13^{\pm 1.01}$	$88.49^{\pm 0.80}$	$37.77^{\pm 2.55}$	$91.39^{\pm 0.52}$
	SubCoOp (Ours)	$27.50^{\pm 2.24}$	$94.63^{\pm 0.30}$	$33.85^{\pm 0.50}$	$92.89^{\pm 0.27}$	$38.46^{\pm 1.00}$	$91.42^{\pm 0.37}$	$47.57^{\pm 2.29}$	$88.77^{\pm 0.62}$	$36.85^{\pm 1.51}$	$91.93^{\pm 0.39}$
RN-50	SCT	$40.33^{\pm 1.25}$	$91.83^{\pm 0.12}$	$36.43^{\pm 1.10}$	$91.65^{\pm 0.19}$	$43.78^{\pm 1.36}$	$88.15^{\pm 0.43}$	$37.62^{\pm 0.93}$	$90.36^{\pm 0.16}$	$39.54^{\pm 1.16}$	$90.50^{\pm 0.23}$
	SubCoOp (Ours)	$40.09^{\pm 1.08}$	$92.21^{\pm 0.14}$	$36.12^{\pm 0.96}$	$91.74^{\pm 0.22}$	$43.08^{\pm 1.41}$	$88.63^{\pm 0.73}$	$37.51^{\pm 0.53}$	$90.31^{\pm 0.13}$	$39.20^{\pm 1.00}$	$90.72^{\pm 0.30}$

FPR95 of 25.85% but slightly higher AUROC of 93.98%. Extremely low value λ_3=0 or high value λ_3=1.0 results in degraded performance.

Figure 13 shows the sensitivity analysis of SubCoOp under different hyperparameter settings. We vary λ_1 and λ_2 while fixing $\lambda_3 \in \{0.2, 0.25, 0.3\}$ and report the FPR95 performance for $C = 100$ and $C = 200$. SubCoOp demonstrates stable behavior across a wide range of configurations, with consistent performance near moderate values of λ_1 and λ_2. This highlights the robustness of our method to different hyperparameter variations.

Table 9 reports the OOD detection performance of various methods on ImageNet-1k under the 1-shot setting using the CLIP-ViT/B-16 backbone. Among prompt-tuning approaches, SubCoOp achieves the lowest FPR95 of 32.18% and the highest AUROC of 91.83%, outperforming the other state-of-the-art baselines across most OOD datasets. The SR-enhanced variants, CoOp-SR and LoCoOp-SR, improve OOD separability compared to their respective baselines. Specifically, CoOp-SR reduces the average FPR95 from 40.80% for CoOp to 38.31% while maintaining a high AUROC of 89.69% compared to 89.77% for CoOp. These results demonstrate that SubCoOp and SR-based enhancements offer consistent gains in few-shot OOD detection over standard prompt-tuning baselines.

Table 11 presents the OOD detection performance of CoOp, LoCoOp, SCT, and the proposed SubCoOp on ImageNet-100 as ID data. SubCoOp achieves the best overall results, with the lowest average FPR95 of 11.60% and the highest average AUROC of 97.80%, consistently outperforming the other methods across all four OOD datasets. While SCT also delivers strong results with FPR95 12.50% and AUROC 97.25%,

Table 7: ID classification accuracy with different baselines(%) utilizing ImageNet-1k dataset

Method	**ID Accuracy**
Zero-shot methods	
MCM	66.7
GL-MCM	66.7
CLIP-based post-hoc methods	
MSP	66.7
ODIN	66.7
Energy	66.7
ReAct	66.7
MaxLogit	66.7
Prompt tuning based methods	
CoOp	71.93
NegPrompt	71.93
SCT	71.72
LoCoOp	71.43
IDlike	71.04
SubCoOp	70.57

Table 8: OOD detection anslysis utilizing ImageNet-1k as ID dataset with varying entropy regularization weights (λ_3).

Method	**iNaturalist**		**SUN**		**Places**		**Texture**		**Average**	
	FPR95↓	AUROC↑	FPR95↓	AUROC↑	FPR95↓	AUROC↑	FPR95↓	AUROC↑	FPR95↓	AUROC↑
SubCoOP (λ_3=0)	16.20	96.67	34.36	93.60	42.19	90.09	43.19	89.43	34.00	92.45
SubCoOP (λ_3=0.1)	12.82	97.28	18.97	95.72	29.62	92.46	41.16	90.69	25.64	94.02
SubCoOP (λ_3=0.3)	15.31	96.59	18.16	96.35	28.89	92.67	41.03	90.61	25.85	93.98
SubCoOP (λ_3=0.4)	15.61	96.58	19.14	95.82	29.38	92.12	40.60	90.51	25.97	93.78
SubCoOP (λ_3=0.5)	14.52	97.08	19.82	95.56	29.94	91.91	42.45	90.27	26.83	93.71
SubCoOP (λ_3=1.0)	15.08	96.71	22.01	94.89	34.00	91.19	44.22	88.91	28.83	92.93

Table 9: Comparison of FPR95 and AUROC scores on various OOD datasets with ID dataset ImageNet-1k. All methods use the same CLIP-ViT-B/16 backbone, and 1-shot training setting.

Method	**iNaturalist**		**SUN**		**Places365**		**Textures**		**Average**	
	FPR95↓	AUROC↑	FPR95↓	AUROC↑	FPR95↓	AUROC↑	FPR95↓	AUROC↑	FPR95↓	AUROC↑
Prompt tuning based methods (1-shot)										
CoOp	$27.99^{\pm 4.18}$	$93.73^{\pm 1.27}$	$36.03^{\pm 4.02}$	$90.95^{\pm 0.57}$	$45.46^{\pm 4.26}$	$87.82^{\pm 1.42}$	$53.70^{\pm 1.79}$	$84.59^{\pm 0.67}$	$40.80^{\pm 3.56}$	$89.77^{\pm 0.98}$
LoCoOp	$26.81^{\pm 2.78}$	$94.45^{\pm 0.72}$	$26.16^{\pm 1.13}$	$94.06^{\pm 0.21}$	$35.18^{\pm 1.05}$	$91.10^{\pm 0.13}$	$50.53^{\pm 0.33}$	$86.96^{\pm 0.60}$	$34.67^{\pm 1.32}$	$91.64^{\pm 0.42}$
IDLike	$12.07^{\pm 0.88}$	$97.65^{\pm 0.10}$	$40.55^{\pm 5.84}$	$91.07^{\pm 1.80}$	$47.94^{\pm 5.24}$	$88.31^{\pm 2.05}$	$38.34^{\pm 13.39}$	$89.67^{\pm 4.03}$	$34.72^{\pm 0.80}$	$91.67^{\pm 0.07}$
NegPrompt	$65.03^{\pm 8.69}$	$84.56^{\pm 2.52}$	$44.39^{\pm 1.66}$	$89.63^{\pm 0.66}$	$51.31^{\pm 6.21}$	$86.55^{\pm 2.19}$	$63.76^{\pm 3.02}$	$83.76^{\pm 3.02}$	$62.08^{\pm 3.71}$	$81.13^{\pm 1.78}$
LSN	$59.28^{\pm 7.02}$	$87.20^{\pm 3.15}$	$40.15^{\pm 0.82}$	$91.47^{\pm 0.14}$	$46.11^{\pm 1.86}$	$88.74^{\pm 0.57}$	$60.34^{\pm 0.14}$	$88.92^{\pm 0.42}$	$51.47^{\pm 1.53}$	$87.84^{\pm 0.58}$
SCT	$20.77^{\pm 4.12}$	$95.15^{\pm 1.15}$	$24.92^{\pm 2.03}$	$94.17^{\pm 0.53}$	$33.35^{\pm 2.03}$	$91.08^{\pm 0.49}$	$50.28^{\pm 1.18}$	$85.71^{\pm 0.08}$	$32.83^{\pm 2.34}$	$91.53^{\pm 0.56}$
SubCoOp	$20.44^{\pm 4.71}$	$94.96^{\pm 1.01}$	$24.13^{\pm 3.60}$	$94.36^{\pm 0.92}$	$32.45^{\pm 3.02}$	$91.78^{\pm 0.72}$	$50.07^{\pm 1.11}$	$87.15^{\pm 0.08}$	$31.96^{\pm 3.11}$	$91.83^{\pm 0.68}$
CoOp-SR	$23.87^{\pm 4.49}$	$94.88^{\pm 1.32}$	$34.68^{\pm 1.65}$	$90.72^{\pm 0.74}$	$42.86^{\pm 1.14}$	$88.92^{\pm 0.71}$	$51.83^{\pm 1.67}$	$84.25^{\pm 0.31}$	$38.31^{\pm 2.24}$	$89.69^{\pm 0.77}$
LoCoOp-SR	$26.31^{\pm 7.74}$	$94.47^{\pm 1.43}$	$26.13^{\pm 1.89}$	$94.41^{\pm 0.23}$	$34.85^{\pm 1.14}$	$91.26^{\pm 0.28}$	$50.62^{\pm 1.67}$	$87.01^{\pm 0.31}$	$34.48^{\pm 3.11}$	$91.79^{\pm 0.56}$

SubCoOp offers further gains, demonstrating its robustness and effectiveness in few-shot OOD detection.

Table 12 presents both training time and performance comparisons, highlighting the computational efficiency of the proposed method. SubCoOp achieves competitive performance with significantly reduced training cost

Table 10: Comparison of FPR95 and AUROC scores using different few-shot techniques (%) on various OOD datasets with ID dataset ImageNet-1k.

Method	**iNaturalist**		**SUN**		**Places**		**Texture**		**Average**	
	FPR95↓	AUROC↑	FPR95↓	AUROC↑	FPR95↓	AUROC↑	FPR95↓	AUROC↑	FPR95↓	AUROC↑
SCT (1-shot)	$20.77^{\pm 4.12}$	$95.15^{\pm 1.15}$	$24.92^{\pm 2.03}$	$94.17^{\pm 0.53}$	$33.35^{\pm 2.03}$	$91.08^{\pm 0.49}$	$50.28^{\pm 1.18}$	$85.71^{\pm 0.08}$	$32.83^{\pm 2.34}$	$91.53^{\pm 0.56}$
SCT (4-shot)	$22.78^{\pm 1.06}$	$95.01^{\pm 0.56}$	$22.97^{\pm 0.72}$	$95.16^{\pm 0.41}$	$33.10^{\pm 2.01}$	$91.80^{\pm 0.43}$	$44.68^{\pm 2.22}$	$89.12^{\pm 0.68}$	$30.88^{\pm 1.50}$	$92.77^{\pm 0.52}$
SCT (8-shot)	$17.45^{\pm 1.19}$	$96.50^{\pm 0.20}$	$24.23^{\pm 0.23}$	$94.82^{\pm 0.31}$	$33.90^{\pm 0.58}$	$91.69^{\pm 0.19}$	$46.71^{\pm 2.09}$	$88.74^{\pm 0.67}$	$30.57^{\pm 1.02}$	$92.94^{\pm 0.34}$
SCT (16-shot)	$16.14^{\pm 1.81}$	$96.68^{\pm 0.29}$	$21.57^{\pm 1.20}$	$95.23^{\pm 0.26}$	$31.47^{\pm 0.89}$	$91.89^{\pm 0.25}$	$43.75^{\pm 0.56}$	$88.83^{\pm 0.45}$	$28.23^{\pm 1.12}$	$93.16^{\pm 0.31}$
SubCoOp (1-shot)	$20.44^{\pm 4.71}$	$94.96^{\pm 1.01}$	$24.13^{\pm 3.60}$	$94.36^{\pm 0.92}$	$32.45^{\pm 3.02}$	$91.78^{\pm 0.72}$	$50.07^{\pm 1.11}$	$87.15^{\pm 0.08}$	$31.96^{\pm 3.11}$	$91.83^{\pm 0.68}$
SubCoOp (4-shot)	$15.16^{\pm 2.58}$	$96.62^{\pm 0.43}$	$19.55^{\pm 2.06}$	$95.71^{\pm 0.57}$	$29.09^{\pm 0.91}$	$92.54^{\pm 0.23}$	$44.06^{\pm 1.68}$	$89.73^{\pm 0.69}$	$26.96^{\pm 1.81}$	$93.61^{\pm 0.48}$
SubCoOp (8-shot)	$14.65^{\pm 2.62}$	$96.48^{\pm 0.32}$	$18.47^{\pm 0.34}$	$95.88^{\pm 0.07}$	$27.28^{\pm 4.91}$	$93.06^{\pm 1.62}$	$43.22^{\pm 1.22}$	$89.76^{\pm 0.14}$	$25.91^{\pm 2.27}$	$93.80^{\pm 0.54}$
SubCoOp (16-shot)	$12.61^{\pm 1.69}$	$97.28^{\pm 0.38}$	$18.75^{\pm 1.47}$	$95.82^{\pm 0.20}$	$29.45^{\pm 1.66}$	$92.51^{\pm 0.13}$	$41.06^{\pm 1.02}$	$90.65^{\pm 0.25}$	$25.47^{\pm 1.46}$	$94.07^{\pm 0.24}$

Table 11: Comparison of FPR95 and AUROC scores (%) on various OOD datasets with ID dataset ImageNet-100.

Method	**iNaturalist**		**SUN**		**Places**		**Texture**		**Average**	
	FPR95↓	AUROC↑	FPR95↓	AUROC↑	FPR95↓	AUROC↑	FPR95↓	AUROC↑	FPR95↓	AUROC↑
CoOp	$23.70^{\pm 6.29}$	$96.67^{\pm 0.57}$	$21.30^{\pm 6.00}$	$96.53^{\pm 0.51}$	$25.75^{\pm 2.37}$	$95.28^{\pm 0.42}$	$19.39^{\pm 1.27}$	$96.85^{\pm 0.16}$	$22.54^{\pm 3.98}$	$96.33^{\pm 0.42}$
LoCoOp	$11.30^{\pm 10.01}$	$97.99^{\pm 0.46}$	$13.90^{\pm 7.35}$	$96.92^{\pm 0.29}$	$20.57^{\pm 10.13}$	$95.50^{\pm 0.39}$	$17.23^{\pm 8.56}$	$96.16^{\pm 0.52}$	$15.75^{\pm 9.01}$	$96.64^{\pm 0.42}$
SCT	$5.26^{\pm 0.21}$	$98.71^{\pm 0.35}$	$11.21^{\pm 3.20}$	$97.54^{\pm 1.16}$	$16.21^{\pm 4.12}$	$96.47^{\pm 0.78}$	$17.32^{\pm 1.76}$	$96.29^{\pm 0.63}$	$12.50^{\pm 2.32}$	$97.25^{\pm 0.81}$
SubCoOp	$5.03^{\pm 1.93}$	$98.83^{\pm 0.28}$	$9.70^{\pm 0.98}$	$98.03^{\pm 0.23}$	$15.06^{\pm 0.32}$	$96.73^{\pm 0.07}$	$16.59^{\pm 0.58}$	$97.59^{\pm 0.31}$	$11.60^{\pm 0.95}$	$97.80^{\pm 0.22}$

by leveraging subspace geometry of visual features. All experiments were conducted using an NVIDIA Tesla V100 GPU (32GB).

Table 12: Training time comparison across different prompt learning-based OOD detection approaches.

Method	ID/OOD Data Aug.	Training time/epoch	Total training time	FPR95↓	AUROC ↑
CoOp	×	0.52 s	5 h 30 min	37.27	91.81
LoCoOp	×	0.66 s	6 h 10 min	30.02	93.14
SCT	×	0.66 s	3 h 10 min	28.23	93.16
OSPCoOp	✓	2.6 s	11 h 38 min	25.54	94.53
Local-Prompt	✓	6.1 s	24 h 5 min	28.27	93.50
SubCoOp	×	0.67 s	3 h 15 min	25.47	94.07